National Society of Black Physicists XXV Annual Day of Scientific Lectures

and

21st Annual Meeting

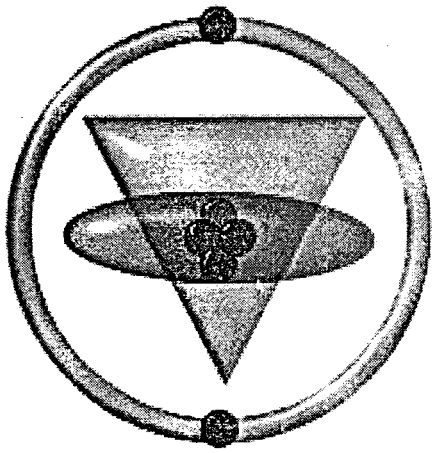

NSBP '98:
"The Next Generation"

March 4-7, 1998
University of Kentucky
Kentucky State University

12th Annual National Conference of Black Physics Students

NCPBS '98:
"Physics/Life in Motion"

March 5-8, 1998
University of Kentucky

JOINT CONFERENCE

DISCLAIMER

This report was prepared as an account of work sponsored by an agency of the United States Government. Neither the United States Government nor any agency thereof, nor any of their employees, makes any warranty, express or implied, or assumes any legal liability or responsibility for the accuracy, completeness, or usefulness of any information, apparatus, product, or process disclosed, or represents that its use would not infringe privately owned rights. Reference herein to any specific commercial product, process, or service by trade name, trademark, manufacturer, or otherwise does not necessarily constitute or imply its endorsement, recommendation, or favoring by the United States Government or any agency thereof. The views and opinions of authors expressed herein do not necessarily state or reflect those of the United States Government or any agency thereof.

DISCLAIMER

Portions of this document may be illegible in electronic image products. Images are produced from the best available original document.

Message to NCBPS and NSBP

We, the National Conference of Black Physics Students (NCBPS), are very pleased to co-convene with the National Society of Black Physicists (NSBP) during our respective annual meetings. This is the 12th consecutive annual meeting of NCBPS. We wish to thank our host institution, the University of Kentucky, Lexington, for giving us the opportunity to join the professional society, NSBP, in celebrating their 25th year.

The goal of NCBPS is to increase the number of Black students obtaining advanced degrees in physics. To this end, our special joint meeting provides us a unique opportunity to establish closer contact with Black Physicists, to broaden mentoring, to provide greater exposure to scientific research, to explore career options with physics degrees and to learn the history of Black contributions to physics. The opportunity to meet with the professiona society does not occur often, full advantage should be taken of this educational meeting.

Dr. Cynthia R. McIntyre, Co-Founder, NCBPS

March 1998

Message from the President

Welcome to the 25th Annual Day of Scientific Lectures and the 21st Annual Meeting of the National Society of Black Physicists. We are extremely proud and happy to be at this point in our existence. NSBP has a rich history. One that is inspirational, that must be told over and over again to a much wider audience. There are young people out there that will find our history "awesome, tight and cool." It is our responsibility to make sure that this rich history is available to inspire all youths: those bright-eyed and questioning, those bold and daring, and those unconcerned and unmotivated.

The Society had its beginnings in the need and desire to recognize, honor and celebrate the work of outstanding Black scientists. As we embark upon this 25th Day of Scientific Lectures, we should view this as a time to celebrate. Many organizations have come and gone in this 25-year period. NSBP has grown and flourished. So let us have a grand celebration during these next two and one-half days.

To help us celebrate, we are very pleased to have the National Conference of Black Physics Students concurrently meeting with us. This is historic, for it marks only the second time that the two conferences have met simultaneously with overlapping events. We extend a hearty welcome to all associated with NCBPS and extend a sincere invitation to join NSBP so that this relationship can continue into the future!

The Society has undergone tremendous change and made significant strides in the 90's. We will recognize and celebrate those accomplishments. We will also begin the process of recognizing and celebrating those individuals who have made significant contributions to NSBP's survival and prosperity. In the midst of the celebrations, we will do what got us where we are today; i.e., good science and good outreach. We will be treated to a full program of interesting talks both theoretical and applied, addressing both old and new problems, by both professionals and students. Again, welcome to NSBP-98. Enjoy the celebration!

Lonzy J. Lewis, President and Chair, NSBP

March 1998

Acknowledgements

The National Society of Black Physicists 1998 Meeting is sponsored by:

The Office of Naval Research
The University of Kentucky:
- Research and Graduate Studies
- Office of Minority Affairs
- College of Arts and Sciences
- Department of Physics and Astronomy

Western Kentucky University

The 1998 National Conference of Black Physics Students is Sponsored by:

National Aeronautics & Space Administration/Kentucky Space Grant Consortium
The National Science Foundation
The US Department of Energy
Oak Ridge National Laboratory
The Southeastern Universities
Research Association
Oak Ridge Associated Universities
The Tennessee Valley Authority
The University of Kentucky:
- Research and Graduate Studies
- Office of Minority Affairs
- College of Arts and Sciences
- Department of Physics and Astronomy

National Student Planning Committe

Alphonse L. Loper, University of Kentucky, Chair
Jamie Valentine, Brown University
Jeremy J. Jackson, Southern University
Clemente Adu, University of Kentucky
G. Y. Ndefru, University of Kentucky
Taravia Taylor, Fisk University

Local Planning Committee/Joint Conference

Alan MacKellar, Chair, University of Kentucky Department of Physics & Astronomy
Lauretta Byars, University of Kentucky Vice Chancellor for Minority Affairs
Dana Cox, University of Kentucky College of Arts and Sciences
Keh-fei Liu, University of Kentucky Department of Physics & Astronomy
Suketu Bhavsar, University of Kentucky Department of Physics & Astronomy
Al Shapere, University of Kentucky Department of Physics & Astronomy
Emmett "Buzz" Burnam, University of Kentucky African American Recruitment Office
Donald Byars II, University of Kentucky Admissions Office
Charles McGruder, Western Kentucky University
Richard Hackney, Western Kentucky University
Karen Hackney, Western Kentucky University

The Local Planning Committee would like to thank the following people for their support:
Carolyn Elery, Pat Tremble, Tony Thomas, Joyce Beatty, Mildred Bailey, Danyel Bell, Charmaine Neal, and Rene Hales

Joint Conference Coordination

Connie S. Blakemore, University of Kentucky International Business & Management Center
Ana Miranda, University of Kentucky International Business & Management Center
Jessika Berry, University of Kentucky
Rene M. Hales, University of Kentucky Media Design & Production

Table of Contents

Conference Papers

Jason S. Best
The Pointwise Dimension Applied to Astronomical Clustering Studies 11

Robert H. Bragg
The Kinetics of Graphitization Revisited: A First Principles Derivation 17

Beth A. Brown
A New View of the X-Ray Emission from Elliptical Galaxies 23

Kenneth A. Brown
VIGILANTE: An Overview of a GPS-based ATR System 31

George Cooper
Molecular and Isotropic Analysis of Organic Compounds from Carbonaceous Meteorites 45

Peter J. Delfyett
Ultra-Highspeed Communications and Data Links Using a Hybrid WDM-TDM Physical Layer 49

F. Hall, IV
The Role of Magnetic Reconnection in the Terrestrial Magnetosphere 55

Wendell T. Hill, III
Atoms and Molecules in Strong Laser Fields 69

Jarita Holbrook
African Astronomy 79

Clifford V. Johnson
Essence of M-Theory 83

Ronald E. Mickens
The Electron 95

H.L. Neal
Teaching Density Functional Theory to Undergraduates 99

Dara Norman
Gravitational Lensing and the Search for Dark Matter 107

F.A. Oguama
Effect of Zn^{2+} Doping on the Phase Transition Temperature of Cadmium Calcium Acetate HexaDrate Single Crystals 111

A.O. Okorogu
Tunable Mid Infrared Downconversion in GaSe and $AgGaS_2$ 121

V.G.J. Rodgers
Yang-Mills, Gravity, and 2D String Symmetries 129

Rony Shahidain
Computer Implementation in Various Physics Courses and Laboratories at Kentucky State University 139

Daniel M. Smith
Workbook for Introductory Mechanics Problem-Solving .....

L. Nan Snow
Why Go to Graduate School?/Successful Admission .....

C.M. Williams
Magnetic and Structural (EXAFS) Properties of Laser Ablated Magnetic Oxide Films .....

ABSTRACTS .....

AGENDAS:

NSBP .....
NCBPS .....

PARTICIPANTS:

NSBP .....
NCBPS .....

CONFERENCE PHOTO .....

NCBPS SURVEY REPORT .....

The Pointwise Dimension Applied to Astronomical Clustering Studies

Dr. Jason S. Best

Shepherd College

Abstract

It can be said that one of the fundamental goals of cosmology is to describe the Universe as accurately as possible. In order to do this, the multiple aspects of the Universe, both past and present-day, must be completely modeled. Some of these characteristics include the age, density, temperature, and extent of the Universe and its components. The modern motivation for fractal geometry may best be summed up by this quote of Benoit Mandelbrot: "Mountains are not cones, clouds are not spheres, coastlines are not circles, and bark is not smooth, nor does lightning travel in a straight line.". Fractals are, in simplest terms, "objects which are (approximately) self-similar on all scales". The renewed modern interest in fractals found as one of its applications the study of the large-scale structure of the Universe, giving a quantitative descriptive scheme to ideas that had been expressed qualitatively as early as C.V.L. Charlier's map of extragalactic nebulae in the 1920s. The focus of this paper will be on results of studies of galaxy catalogs and galaxy cluster catalogs using the pointwise dimension, or PD. The PD is an easy-to-use fractal statistic which has numerous advantages over the more traditional methods used to study the clustering of astronomical objects. It is believed that much new information can be gleaned with this statistic about the environments of the galaxies and of the clusters in these catalogs.

1. Introduction to the Astronomical Issues

Two components of the modern-day Universe that can be analyzed in order to understand its evolution are the clustering of objects in the Universe and the relationship between a galaxy's morphology and its environment.

On the largest scales, the Universe is believed to be everywhere homogeneous and isotropic: this is evidentially verified by such observations as the isotropy of the cosmic microwave background. However, on smaller scales, the universe is certainly not observed to be homogeneous. For instance, the average density of a galaxy is $\sim 10^5$ times that of the Universe, while a cluster's average density is $\sim 10^2$ times that of the Universe (Peebles 1993). Furthermore, galaxies are observed to be distributed not at random, but clustered with respect to each other; the "soap bubbles" of de Lapparent, Geller, and Huchra 1986 are one of the more famous demonstrations of this. Any theory of structure formation must also be able to account for this observed clustering of objects.

Hubble and Humason 1931 demonstrated that the morphological fractions of ellipticals, lenticulars, and spirals are related to the density of the environment. The fraction of ellipticals ranges from less than 10% in the lowest density environments to more than 50% in the centers of galaxy clusters (Dressler 1980a). It is still not apparent whether this is a result of conditions conducive to formation

of a particular morphological type (nature) or to an evolutionary process (nurture). There are multiple scenarios that can account for this "morphological segregation", including scenarios based on star formation rate dependence on the level of the density fluctuation that forms a galaxy (Zurek, Quinn, and Salmon 1988), the stripping of a spiral or lenticular galaxy's disk by tidal or pressure forces in the center of a galaxy cluster (Gunn and Gott 1972), or merger scenarios (Toornre 1977, Hernquist 1980).

It is very difficult to determine which of the various nature and nurture mechanisms dominate. It would appear that the clustering properties of different morphological types should be diagnostic of the formation mechanism, but in practice the distinctions are very subtle. If nature is the motivating factor, then whatever local properties are needed to make ellipticals could tend to exist over a large region. If a nurture mechanism involving mergers is the dominant mechanism, then initial correlations in the positions of spirals could lead to numerous mergers in one region. Thus, in both mechanisms, a correlation between morphology and environment will arise. Whitmore, Gilmore, and Jones 1993 argue for a hybrid model of origin of morphology in which the same fractions of spirals, lenticulars, and ellipticals are set by nature to form everywhere in the Universe.

2. Methods of Analyzing Clustering

The two-point correlation function is the most common way of describing the distribution of galaxies. As defined by Peebles 1980, the two-point spatial correlation function $\xi(r_{12})$ can be written as

$$\delta P = n^2 \delta V_1 \delta V_2 [1+\xi(r_{12})] \qquad (1)$$

where n is the galaxy number density, and δP is the joint probability of finding an object in both volumes δV_1 and δV_2 at separation r_{12}. It is convenient to compute ξ as

$$\xi(r_{12}) = (N_{real} / N_{rand}) - 1 \qquad (2)$$

where N_{real} is the number of galaxy pairs in the observed sample with separations between r and $r + \Delta r$, and N_{rand} is the number of pairs in the same interval for the same number of galaxies distributed randomly over an identical volume.

The two-point correlation function, how shows some limitations when providing complete description of galaxy distribut major problem is that the technique ass that the galaxy distribution becomes spa homogeneous on a length scale that is sr than that of the catalog being analyzed. assumption is invalid, the amplitude of t correlation function and the length scale where the function becomes small are sa dependent (Pietronero 1987). The two-pc correlation function is also limited in tha averages together amplitudes on a given that come from galaxy pairs in many diff environments. This can yield a large amplitude for $\omega(\theta)$ because there are a lar number of close neighbors for a small fra of the galaxies in the sample or because o smaller number of neighbors for nearly ai galaxies in the sample. In other words, wh the two-point correlation function indicat that the galaxies are correlated, it does no reveal the number of galaxies that contrib to give the value. Finally, this statistic is m often applied either to all galaxies in a sam or to galaxies of the same morphology (e.g. elliptical-elliptical pairs) . Some environmental influences on morphology might have more to do with the total numb of galaxies in the environment of a particul type.

Observational determinations of the correlation function $\xi(r)$ yield a relationship of a power law form

$$\xi(r)=Br^{\gamma}$$

which has been determined to have a nearly constant slope over more than two orders of magnitude in distance (from galactic scales galactic cluster scales). This behavior for object clustering suggests that the concept o fractal geometry may apply (Mandelbrot 1983, Peebles 1993). The modern motivation for fractal geometry may best be summed up by this quote: "Mountains are not cones, clouds are not spheres, coastlines are not circles, and bark is not smooth, nor does lightning travel in a straight line." (Mandelbrot 1983). Fractals are, in simplest terms, "objects which are (approximately) self-similar on all scales". Imagine a cauliflower having a piece broken off: that piece resembles a miniature cauliflower. This is an example of self-similarity.

The pointwise dimension, or PD, is particularly useful for analyses of correlations between morphology and environment. It also has the distinction of being conceptually simple and easy to apply to two- and three-dimensional object catalogs.

I can consider a function $N_{\vec{x}_m}(r)$ which is the count of the number of data points within a distance r from a reference point $\vec{x}_m$. In a log-log representation, there is a scaling region over which a slope can be defined; within that scaling region, which is bounded by r_{min} and r_{max}, this slope $d_{\vec{x}_m}$ is interpreted as the pointwise dimension, and is defined as (Mayer-Kress 1994)

$$d_{\vec{x}_m} = \frac{log(N_{x_m}(r_{max})) - log(N_{x_m}(r_{min}))}{log(r_{max}) - log(r_{min})} \qquad (4)$$

In other words: one can characterize the environment of an object (known as the primary: it can be a galaxy, galaxy cluster or indeed any object the environment of which we wish to describe) by calculating how the number of objects surrounding the primary (the surrounding objects are known as secondaries) changes as a function of distance from the object. The maximum distance from the primary out to which we choose to calculate the slope is known as the "fitting range".

This research has two ends. First, I am attempting to quantify clustering of astronomical objects via the pointwise dimension. Second, I am trying to, when possible, study the possible relation between a galaxy's morphology and its complete environment.

3. Description of Data

The pointwise dimension has been used by this author to study a variety of catalogs. Three such catalogs are the RC3, the Dressler catalog, and the ACO.

The Third Reference Catalog of Bright Galaxies, or RC3 (de Vaucouleurs 1991), has been studied in a previous paper by this author (Best, Charlton, and Mayer-Kress 1996). The total number of galaxies in the catalog is 23,024, and it is complete for galaxies of apparent diameters greater than 1 aremin, B-band magnitudes brighter than 15.5, and radial velocities less than 15,000 km/s. For these analyses, we considered only a subsample of the catalog, where each galaxy needed to have either an apparent diameter of greater than 1 arcmin, or a B magnitude brighter than 15.5. This reduced the number to just under 22,000. In order to apply the analyses to the largest continuous areas possible (to avoid boundary effects), we analyzed the northern and southern hemispheres as separate populations. Boundaries of ±20 degrees galactic latitude were also used in order to avoid the galactic dust lane and an area of undersampling in the catalog. There remained 10493 galaxies in the northern sample and 8560 in the southern sample. Among the conclusions of that work were: 1) The PD elucidates the tendency for early-type galaxies to cluster more than late-type galaxies; however, there is considerable overlap between these populations. 2) The pointwise dimension, or PD statistic, does not find a significant relationship between luminosity and clustering in RC3, but it could be an effective diagnostic in larger 2D catalogs. 3) The majority of galaxies in RC3 (excluding clusters) are spread out in space much like a random distribution.

PD analyses have also been conducted on Dressler's 1980 catalog of morphological types in 55 rich clusters of galaxies (Dressler 1980b). Dressler's main selection criteria were cluster richness (a measure of the number of galaxies within the cluster), low redshift (a measure of the distance of the cluster from the observer), and containment and definition within a few square degree area of the sky. In this catalog, the smallest number of galaxies in a cluster is 44 and the largest cluster redshift is ~0.064. Dressler took from the Abell Catalog (Abell 1958) 38 clusters, and completed the catalog with 17 previously unstudied clusters, which were obtained "...from a rather complete inspection of a plate copy of the ESO Quick Blue Survey". Dressler considers the overall quality of the data "good to excellent".

The catalog contains, for each cluster galaxy (~6000 galaxies in all), information on its position, morphology, apparent visual magnitude, estimated bulge size, and ellipticity. Dressler also lists a redshift for each cluster. The characteristics most

immediately relevant to my PD analyses of this catalog are redshift and morphology. Redshifts had been previously obtained for 26 of the clusters between 1973-1979 by other observers. Dressler used the du Pont telescope to obtain redshifts for at least two galaxies per cluster for each of the other clusters.

Morphological classifications for galaxies are determined by Dressler via the following criteria. Ellipticals have smooth radial profiles, and no intensity discontinuities. Lenticulars contain a non-spheroidal component, or an intensity discontinuity between the bulge and disk. Spirals show either disks with clear spirals or outer rings, or dust lanes extending through the disk length. Irregulars are amorphous dusty objects, while the Unclassified category contains anything not contained in the first four categories. Dressler also allows for transition cases. Transitions between ellipticals and lenticulars are discriminated by intensity discontinuities, while transitional spiral/lenticular cases are assigned due to uncertain detection of spiral structures.

The ACO Catalog (Abell, Corwin, and Olowin 1989) is the largest all-sky cluster catalog currently available to the public, and thus makes a good candidate for a PD study. The ACO catalog contains 4073 rich clusters of galaxies, each having at least 30 members within a magnitude range m_3 to m_3+2 (where m_3 is the magnitude of the third brightest member of the cluster). As well, the 1989 sample had nominal redshifts less than 0.2. The authors claimed completeness to this level; however, a detailed analysis by Scaramella 1991 proved that the catalog is truly complete only to a redshift of 0.1. Consequently, that value will be used as the completeness threshold in PD analyses of this dataset. The catalog also contains information on position, richness class (the number of clusters not more than two magnitudes fainter than the third brightest cluster), distance class, V magnitude, and apparent cluster center. The catalog is separated into a northern and a southern catalog by the ACO authors, with northern being Abell's original catalog and southern being the 1989 completion. The combined catalogs have been divided by this author with respect to the galactic equator. From this point onward, unless specifically noted, the northern ca contains those galaxies north of the galac equator, while the southern catalog refers those galaxies south of the galactic equat

Since I wished to do a three-dimensional analysis, redshift information was desirab In some cases, a redshift had been determ previously. In some cases, information on redshifts was obtained from the ESO Nearl Abell Cluster Survey, or ENACS (Katgert 1996), which studied 5634 galaxies in the direction of 107 clusters from the ACO catalog. The authors of that paper conclu that "...we do not find systematic velocity offsets [between ENACS data and previous published work] at a level which would prevent a useful combination between our data and those from the literature" (Katge 1996). This being the case, the ENACS reds information has been incorporated into th PD analyses when no other redshift data w available.

4. Three-dimensional ACO Analysis

This paper will focus on a single result of t research: the large-scale clustering extent the ACO catalog. A 3D analysis of the ACO subsequently been undertaken. A Hubble f with no deviations is used to get a distance each cluster. This distance, along with the galactic latitude and galactic longitude, car used to convert into a 3D distribution usin standard spherical coordinate transformations.

Aside from the dust lane boundary in effec 3D analysis must take another boundary in account. In spherical polar coordinates, a distribution of points (galaxies, clusters, et with a galactic latitude cutoff has a bounda defined by a trigonometric function of that cutoff (the function is unimportant; it is enough to know that it exists) I as well as a outer edge due to the lack of galaxies past t limiting redshift. Both boundaries are taker into consideration before a cluster is considered as a primary for a particular fitting range. The outer edge of the data has been set to a distance corresponding to a redshift of 0.1. The fitting ranges chosen we 0-10, 0-25, 0-50, 0-100, and 0-200 Megaparsecs (Mpc).

What I actually want to know, if possible, is the following: is the true distribution of clusters in the Universe random on large scales, or does it differ significantly from that of a random distribution? The best case scenario would be to have an all-sky catalog to answer this; this would give you a maximum extent. This is nearly the situation present here (only the galactic plane boundary imposed prevents this). For each hemisphere, one can compare the real data to a 3D random catalog, since on the scales of interest there should be little effect from velocity dispersions.

5. Discussion and Conclusion

Incorporating a minimum galactic latitude boundary of ±20 degrees (to avoid the galactic dust lane) and a redshift maximum of 0.1, the ACO cluster and random catalog distributions are compared directly using a KS (or Komolgorov-Smirnov) two-distribution test for both the northern and southern galactic hemispheres. This test is designed to determine to what significance we can say that the two distributions are or are not drawn from the same parent distribution. For both hemispheres, in all but one case the distribution of PDs for the random catalog and the ACO catalog are not similar to the 99th percent level using a KS test. That one case is the largest fitting range: that of 200 Mpc. This means that on scales below 200 Mpc, the ACO and random catalogs are not statistically similar to the 99th percent level.

Unfortunately, there were not enough data in the 25 Mpc fitting range of either the northern or southern random catalog to get a comparison to the "cluster correlation length" of 25 Mpc (Bahcall and Soneira 1983). However, in the range 0-50 Mpc, which is the first range for which there are enough data to compare ACO and Random results, the northern and southern distribution of the PDs from the ACO significantly differ from the randomly distributed PDs to the 99% level, and their median PDs and error bars do not overlap significantly.

I note that clustering on scales greater than the cluster correlation length has been found by other authors (Bahcall 1993, Borgani, Plionis, and Valdarnini 1993, Pietronero, Montuori, and Sylos Labini 1997, Sylos Labini, Pietronero, and Montuori 1997). Bahcall goes as far as to say that "The universal dimensionless cluster correlation function is consistent with a fractal structure in the distribution of clusters". She also notes that the ACO catalog is consistent with this picture. This does not rule out homogeneity on the largest scales; this does, however, push the cluster correlation length scale up quite a bit. In fact, it is found that the random catalogs' 3D PD values are not always 3.0, the value expected for a homogeneous distribution. This is to be expected, since a random catalog is not necessarily a homogeneous catalog on all scales. In fact, we should expect some small-scale clustering in a random catalog. The argument is, or should be, as to whether or not the Universe is homogeneous not on all scales but on the largest scales. Even proponents of the cosmological principle (CP) will admit that the structure seen in the Universe eliminates the possibility of a universe homogeneous on all scales (Davis 1997). What this research results in is not a denial of the CP. It is argued only that on the scales of the ACO catalog, we still see a structure that would be significantly different than that of a homogeneous catalog on the majority of scales probed. It is also noted that Kerscher 1997 finds that "the scale of homogeneity is considerably larger than $200h^{-1}$Mpc". These authors used an alternative method on the IRAS 1.2 Jy catalog. Sylos Labini, Pietronero, and Montuori 1997 claim structure on scales even larger than this from pencil-beam studies. Of course, these studies take into account only luminous matter. Dark matter, distributed homogeneously on large scales would of course gravitationally dominate on those scales. It is also quite possible that we may have not yet probed deep enough to see homogeneity. Evidence for a fractal distribution in COBE data (de Gouveia Dal Pino, Hetem, and A. de Araujo 1995) further adds to the possibility that while homogeneity may be the actuality, it may not occur until scales much greater than previously thought.

References

Abell, G. O. 1958, *ApJS*, **3**, 11.

Abell, G. O., Corwin, H. G., and Olowin, R. P. 1989, *ApJS*, **70**, 1.

Bahcall, N. 1993, *Proc. Natl. Acad. Sci. USA*, **90**, 4848.

Bahcall, N. and Soneira, R. M. 1983, *ApJ*, **270**, 20.

Best, J., Charlton, J., and Mayer-Kress G 1996, *ApJ*, **456**, 55.

Borgani, S., Plionis, M., and Valdarnini, R. 1993, *ApJ*, **404**, 21.

Davis, M. 1997, in *Critical Dialogues in Cos-mology*, (Princeton: Princeton University Press).

de Gouveia Dal Pino, Hetem, E. M., and A. de Araujo, J. 1995, *ApJ*, **442**, 2.

de Lapparent, V., Geller, M., and Huchra, J. 1986, *ApJL*, **302**, L1.

de Vaucouleurs, G. e. a. 1991. *Third Reference Catalog of Bright Galaxies*, 1. (New York: Springer-Verlag).

Dressler, A. 1980a, *ApJ*, **236**, 351.

Dressler, A. 1980b, *ApJS*, **42**, 565.

Gunn, J. and Gott, J. 1972, *ApJ*, **176**, 1.

Hernquist, L. 1980. *The Environment and Evolution of Galaxies*, 327. eds. J.M. Shull, H.A. Thronson Jr. (Dordrecht: Kluwer Academic Publishers).

Katgert, P. e. a. 1996, *A&A*, **310**, 8.

Kerscher, M. e. a. 1997, in *Proceedings of the Workshop "Astro-particle physics"*, (held in Ringberg Castle Oct 10-15 1996), in preparation.

Mandelbrot, B. 1983. *The Fractal Geometry of Nature*, Chapter 1. (New York: W.H. Freeman and Company).

Mayer-Kress, G. 1994, *Integrative physiologi-cal and behavioral science*, **29**, 203.

Peebles, P. J. E. 1980. *The Large-Scale Struc-ture of the Universe*, 143. (Princeton: Princeton University Press).

Peebles, P. J. E. 1993. *Principles of Physical Cosmology*, Section 1. (Princeton: Princeton University Press).

Pietronero, L. 1987, *Physica*, **114a**, 257.

Pietronero, L., Montuori, M., and Sylos Labini, F. 1997, in *Critical Dialogues in Cosmology*, (Princeton: Princeton Uni-versity Press).

Scaramella, R. e. a. 1991, *AJ*, **101**, 342.

Sylos Labini, F., Pietronero, L., and Montuori, M. 1997. *Proceedings of the Workshop "Astro-particle physics"*, chapter in preparation. (held in Ringberg Castle Oct 10-15 1996).

Toomre, A. 1977. *The Evolution of Galax-ies and Stellar Populations*, 401. eds. B. Tinsley, R. Larson (New Haven: Yale Univ. Obs.).

Whitmore, B., Gilmore, D., and Jones, C. 1993, *ApJ*, **407**, 487.

Zurek, W., Quinn, P., and Salmon, J. 1988, *ApJ*, **330**, 519.

The Kinetics of Graphitization Revisited: A First Principles Derivation

Robert H. Bragg

T. E. Glover

University of California, Berkeley

Abstract

Graphitization has been modeled as a solid state chemical reaction involving four metastable graphite self-interstitial compounds wherein phase i transforms to phase i-1 with rate constants $k_i = \overline{K}_i \exp(-E_i/kT)$. The solution of the corresponding set of coupled linear first order ordinary differential equations, combined with the corresponding interlayer spacings, 0.355 nm, 0.344 nm, 0.340 nm, and 0.3375 nm provides an expression that describes the time-temperature history of the annealing process. Results of E_i obtained using literature data are E_1 = 7.46 eV, E_2 = 5.81 eV, E_3 = 4.55 eV, and E_4 = 3.36 eV. Within experimental error E_1 matches the heat of sublimation of graphite, and E_4 is equal to the activation energy for a-direction vacancy migration in graphite.

I. Introduction

Many studies of the conversion of carbon materials to graphite by high temperature isothermal annealing of soft carbon have employed X-ray data of the apparent interlayer spacing d_{002} in the equation[1,2]

$$d_{002}=d=d_0+(d_1-d_0)\exp(-k_1t)+(d_2-d_1)\exp(-k_2t) \qquad (1)$$

where d_0 = 0.3354 nm, d_1 = 0.338 nm and d_2 = 0.344 nm, and $k_i = K_i \exp(-E_i/kT)$. The form of this equation seems to be appropriate for describing the annealing process for a variety of structure sensitive properties, e.g., diamagnetic susceptibility and the Hall coefficient. However, the calculated value of E_i often exceeds the heat of vaporization of graphite, and it is usually necessary to resort to a distribution of rate constants to obtain a reasonable fit of the data. Typical annealing data are shown in Fig. 1.

Equation (1) has not heretofore been obtained from a first principles derivation. There is no reason, *a priori*, to assume only one or two E_i's, especially since the rate of annealing at a given temperature decreases as the *extent* of annealing increases, i.e., the closer d approaches d_0. The model of Maire and Mering of turbostratic graphite provides a promising alternative to the intuitive approach just described.[3] In this model there are four metastable graphite self-interstitial compounds, and a given carbon may contain a mixture of all, and in addition of course, graphite. Bragg and co-workers have presented strong evidence in support of this model,[4] and in fact assign the values d_4 = 0.355 nm, d_3 = 0.344 nm, d_2 = 0.340 nm, and d_1 = 0.3375 nm to the interlayer spacings of these phases. With this refinement the process of graphitization is simply the sequential transformation from phase i to phase i-1 with rate constant $k_i = \overline{K}_i \exp(-E_i/kT)$. In this work the appropriate set of differential equations is set up, solved and tested with available literature data.

II. Derivation

A. The reaction kinetics

We assume that a general starting carbon material prior to annealing is a mixture of phases whose volume fractions are $x_i = x_i(t)$, where $\Sigma x_i=1$. During annealing the set of

simultaneous equations that describes the process is

$$\left.\begin{aligned} \frac{dx_1}{dt} &= -k_4 x_4 \\ \frac{dx_3}{dt} &= -k_3 x_3 + k_4 x_4 \\ \frac{dx_2}{dt} &= -k_2 x_2 + k_3 x_3 \\ \frac{dx_1}{dt} &= -k_1 x_2 + k_2 x_2 \\ \frac{dx_0}{dt} &= k_1 x_1 \end{aligned}\right\} \qquad (2)$$

where $k_i = \overline{K}_i \exp(-E_i/kT)$, and at $t = 0$, $x_i = \overline{X}_i(0)$. Since $x_i(t) = 1$, it follows that $\sum x_i(t)=1$, $\sum \overline{X}_i(0)=1$. The solution of Eqs. (2) can be obtained by standard techniques of ordinary differential equations. The expressions for the $x_i(t)$ are a big lengthy and are not shown here. However, if $x_4 >> x_3 >> x_2 >> x_1$, then the results are simpler and are used later in this paper.

B. The significance of d_{002}

If the d_{002} X-ray lines of the constituent phases were resolved the amounts of these phases could be determined using the fact that the integrated intensity I_i of a characteristic peak of the i_{th} phase is given by

$$I_i = I_0 Q_i V_i \qquad (3)$$

Where I_0 is the incident beam intensity, Q_i is the reflecting power per unit volume and V_i is the volume of phase i. However, the peaks of the component phases partially overlap because the nominal peak separations, about 0.1 to 0.5 degrees 2θ, are comparable to the line breadths (due to small crystallite size) of these peaks, as shown in Fig. 2. Thus the appropriate parameter to characterize the distribution of peaks is the centroid $<2\theta>$. Now for each component i, whose line profile is $P_i(2\theta)$,

$$\int_{-\infty}^{\infty} P_i(2\theta)d2\theta = I_i; \quad \int_{-\infty}^{\infty} 2\theta P_i(2\theta)d2\theta = <2\theta>$$

here $<2\theta>_i$ is the centroid of peak i. The profile of the mixture is the sum of the components,

$$P(2\theta) = \sum P_i(2\theta)$$

With Eq. (3), Eq. (4) and Eq. (5) one find the centroid $<2\theta>$ of the mixture is

$$<2\theta> = \sum <2\theta>_i I_i / \sum I_i$$

And with the assumption that $Q_i = Q_j = Q$ (6) can be rewritten

$$<2\theta> = \sum <2\theta>_i x_i$$

where $x_i = V_i / \sum V_i$ is the volume fraction c i^{th} phase.

C. The connection to annealing kinetics

By combining Eq. (7) with the solutions of Eqs. (2) one obtains a very lengthy expression. If we make the assumption, justified *a posteriori*, that $k_i >> k_i$-1, then a much simpler expression is obtained. If we further note that over the narrow range of spanned by a composite peak the *differen* in 2θ are a linear function of the *differenc* in the corresponding d's, then the annealir kinetics are represented by

$$\begin{aligned} <d> = d_0 &+ \{d_1 - d_0\}\{\overline{X}_1(0) + \overline{X}_2(0) + \overline{X}_3(0) + \overline{X}_4(0)\}\exp(-k_1 t) \\ &+ \{d_2 - d_1\}\{\overline{X}_2(0) + \overline{X}_3(0) + \overline{X}_4(0)\}\exp(-k_2 t) \\ &+ \{d_3 - d_2\}\{\overline{X}_3(0) + \overline{X}_4(0)\}\exp(-k_3 t) \\ &+ \{d_4 - d_3\}\{\overline{X}_4(0)\}\exp(-k_4 t) \end{aligned} \qquad (8$$

III. Test of Eq. (8)

A proper test of Eq. (8) requires annealing data wherein <d> or $<2\theta>$ was measured, bu heretofore data have been reported only fo: the peak position $\hat{d}$. Figure 2 shows a (004) line profile obtained from a thin plate of pyrolytic carbon which has been decompose into its component peaks. Note that the peal at 0.355 nm makes a significant contributio

to the centroid, but only a small contribution to $\hat{d}$. Thus by setting $d_4 = 0$ in Eq. (8) one can use the literature data taking $\langle d \rangle \approx \hat{d}$ to a good approximation. Data of Figs. 4, 16 and 19 of Reference (1) were fitted using Eq. (8) with d_4 set equal to zero. The best fit using all of these data gave

i	E_i,eV	$\bar{K}_i$,min^{-1}
1	7.46	1.1×10^8
2	5.81	2.8×10^7
3	4.55	6.0×10^6
4	3.36	0.7×10^4

IV. Discussion

Equation (8) evidently contains Eq. (1) as a very special case, and it also explains why different investigators obtain annealing data that differ at the lowest annealing temperatures, but they are all very similar for large T and long t. It is also clear that one cannot bring a carbon to a standard state by preliminary anneals. The results are very preliminary but very encouraging, especially the results obtained for E_1 and E_4. For purposes of comparison, the heat of vaporization of graphite is 7.41 eV and the activation energy for vacancy migration, a-direction in graphite, is 3.10 ± 0.20 eV. The authors have no proposal for the mechanism corresponding to E_2 and E_3.

One implication for future research is that investigators should measure line profiles instead of peak positions. With such data one obtains the x_i directly from peak decomposition analysis, and in addition from $\langle d \rangle$ the validity of Eq. (8) can be tested. To the extent that Eq. (8) is corroborated, it will be possible to predict the entire course of the annealing process from one X-ray measurement.

References

[1]D. B. Fischbach, Chemistry and Physics of Carbon **7**, 71 (1971).

[2]A. Pacault, Chemistry and Physics of Carbon **7**, 107 (1971).

[3]J. Maire and J. Mering, Chemistry and Physics of Carbon **6**, 125 (1970).

[4]J. Lachter and R. H. Bragg, Phys. Rev. B **33**, 893 (1987).

FIG. 1. The unit-cell height c = 2d as a function of the logarithm of isothermal HTt at various temperatures for a pyrolytic carbon.

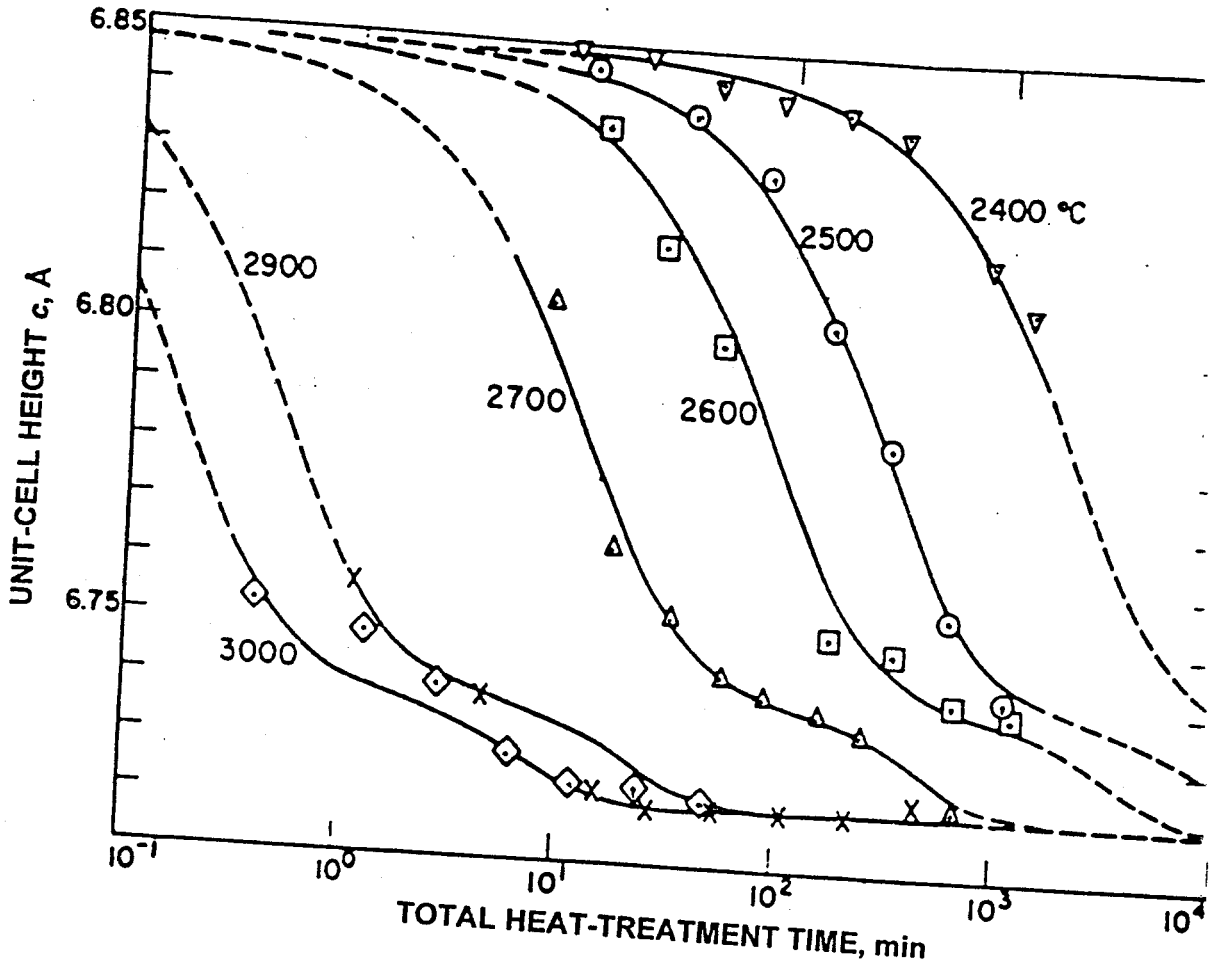

Figure 1. The unit-cell height c=2d as a function of the logarithm of isothermal HTt at various temperatures for a pyrolytic carbon.

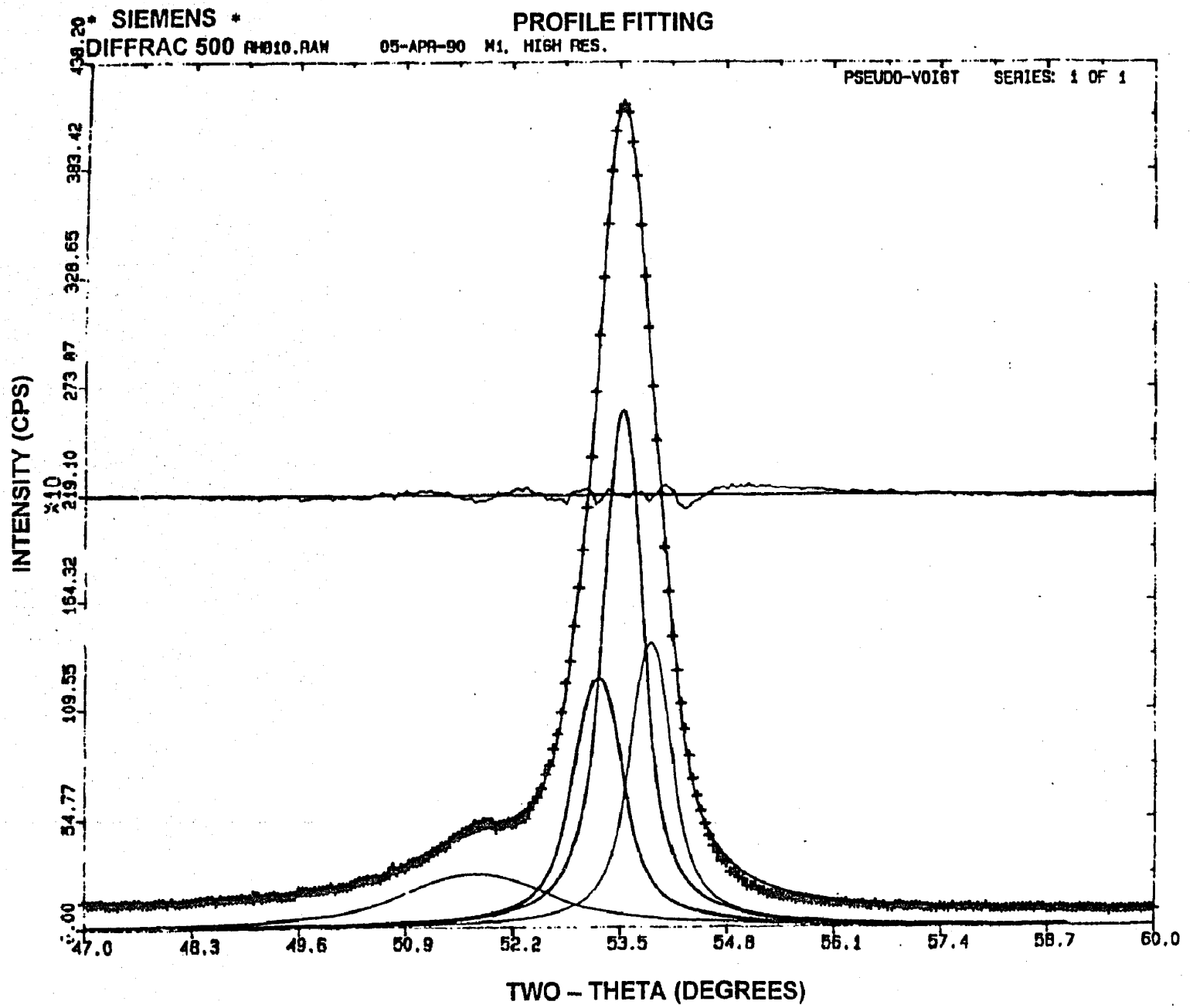

Figure 2. (064) line profile of as-received pyrolytic carbon showing profiles of component phases.

A New View of the X-Ray Emission from Elliptical Galaxies

Beth A. Brown

University of Michigan

Abstract

We have obtained an optically flux-limited sample of 34 elliptical and SO galaxies, observed with high and low angular resolution detectors on the X-ray Röntgen Satellite (ROSAT). The survey is large enough to test the present picture of cooling flow models developed to explain the origin, behavior, and evolution of hot gas found to be present in elliptical galaxies. For this sample of galaxies, we have established well-defined X-ray luminosities, and have determined X-ray gas temperatures for a subset of the survey. A steep relationship is found between the X-ray and optical luminosities with a slope of 2.72±0.27, with a large dispersion about the correlation. We confirm a correlation between the X-ray temperature (T_x) and stellar velocity dispersion temperature (T_σ), with $T_X \propto T_\sigma^n$ where n = 1.43±0.21. We also find X-ray gas temperatures 2 - 3 times hotter than expected for some galaxies. The results are inconsistent with predictions of the standard cooling flow model for elliptical galaxies, and we suggest a modification of the model that places environment in a central role in determining the X-ray emission properties. In our model, early-type galaxies attempt to drive partial or total galactic winds, which can be stifled by the pressure of their environment. Stifled winds should lead to hotter and higher luminosity systems, which would occur most commonly in the richest environments, as observed.

1. Introduction

The *Einstein Observatory* discovered that some early-type galaxies are powerful emitters of X-rays, and that their X-ray luminosity is correlated with their optical luminosity (Forman, Jones, & Tucker 1985; Canizares, Fabbiano, & Trinchieri 1987). It also showed that the temperature of the hot gas is approximately that expected for gas that is gravitationally bound to the system. For the more luminous X-ray-emitting ellipticals, where we are confident that the X-ray emission is dominated by the hot gas, the current model posits that gas is lost by stars through normal stellar evolution and is subsequently thermalized in the potential well of the galaxy, or heated by supernovae (e.g., Sarazin 1990). The gas then radiatively cools (producing the X-ray emission), and slowly flows into the center of the galaxy.

The existing picture makes certain predictions, such as that the X-ray luminosity should be proportional to the mass loss rate of stars and the depth of the potential well (approximately L_x *oc* $L_B^{1.7}$), with modest dispersion, and that the temperature of the hot gas (T_x) should be proportional to the stellar velocity dispersion (σ) squared. Studies with the *Einstein Observatory* led to luminosity relationships that were either consistent with or steeper than the expected L_X - L_B slope, but with considerable dispersion about the best-fit line (Canizares, Fabbiano, Trinchieri 1987; Donnelly, Faber & O'Connell 1990; White & Sarazin 1991; Bregman et al. 1992; Kim et al. 1992). The *Einstein Observatory* did not provide accurate temperature information for comparison with the velocity dispersion. The Röntgen Satellite (*ROSAT*), with a factor of two improvement in spectral resolution, does permit accurate

determinations of gas temperature. The first published *ROSAT* sample is that of Davis and White (1996), who found a correlation between X-ray temperature and stellar velocity dispersion, with temperatures greater than anticipated. Here we present X-ray luminosities from our complete survey of optically selected elliptical galaxies, and temperatures for a subset of the sample. An extensive discussion of the sample, data processing techniques, and additional statistical analysis of the sample appear elsewhere (Brown 1998).

2. Sample Selection and Flux Determinations

The primary goal was to define an unbiased sample of early type galaxies for which a complete set of X-ray data could be obtained. We chose an optically-selected flux-limited sample of galaxies based upon the work of Faber et al. (1989), who obtained a consistent set of distances for these galaxies. This is essential for accurately establishing the L_X - L_B relationship and defining the scatter about the relationship.

The number of galaxies in the sample is a compromise between the desire to have many targets while avoiding many upper limits in the sample. Based upon the L_X - L_B relationship from the *Einstein Observatory,* we estimated that the percentage of detectable galaxies decreases significantly beyond the 30 - 40 optically brightest galaxies, for sensible exposure times with the PSPC or HRI on *ROSAT.* With 30 - 40 objects, calculations showed that we should be able to define the L_X - L_B relationship with sufficient accuracy to discriminate between competing models. Our final sample (Table 1) is comprised of the 34 optically brightest early-type galaxies in Faber et al. (1989) with $|b| > 20°$, while avoiding dwarf galaxies (e.g., NGC 185, NGC 205, NGC 221) and X-ray bright quasars (e.g., M87). X-ray data for about two-thirds of the sample were obtained from archival sources, with the remainder specifically observed for this project.

It is unclear how to best choose the region within which to define the X-ray emission from ellipticals because the flux increases logarithmically with radius for a typic surface brightness distribution. We ha chosen to define the flux within an op defined radius since we are trying to t models related to the galaxy (e.g., mas from the stars). We extract our signal radius of $4r_e$, (r_e is de Vaucouleurs hal radius), within which 85% of the optic is contained. The background is taken between 4-6.3r_e for all galaxies, which removes the X-ray emission surroundi galaxy, while maximizing the signal-to- This method creates a very well define this sample, although we recognize the be an underestimation of the flux in so galaxies. For a few galaxies, such as the weakest sources observed with the HRI, signal is defined within 1r_e and extrapc to 4r_e to maintain consistency within th sample.

Raymond-Smith thermal plasma model fit to X-ray spectra, under the assumpti fixed metallicity of 50% solar and adopt the Galactic neutral hydrogen density c (N_H, fixed for each galaxy), which is acc to about 5% (Hartmann & Burton 1997) northern hemisphere and to about 10% southern hemisphere (Dickey & Lockma 1990). For the 19 PSPC galaxies with enc photon counts to constrain the tempera (generally, >300 counts), a single-tempe model was fit. If the resulting x^2 was unacceptable, a two-temperature model subsequently fit, with a "hard" compone whose temperature was fixed at 2 keV (presumably, reflecting a stellar binary contribution); the softer component is assumed to be from the hot gas.

For the extraction of the flux, we used ei the fitted temperatures or, for objects wi few counts, we usually assumed $T_X = 1.5$ a few objects with very low values of 1.5 minimum temperature of 0.3 keV was assumed, since lower temperatures were clearly a poor fit, even for objects with o 100 counts. We note that the luminositie nearly independent of the metallicity assumed, and the temperatures have a m dependence on the metallicity (for a metallicity that differs by a factor of two our adopted value, the temperature chan by 10% or less).

3. Analysis and Interpretations

There can be a large correction to the flux from 0.1 - 0.5 keV due to Galactic absorption, so we will focus our discussion on the luminosities determined for the 0.5 - 2.0 keV band which is fairly insensitive to Galactic absorption corrections. A logarithmic plot of L_B (derived from Faber et al. 1989 magnitudes) against L_X is shown in Figure 1. Also included on the plot are stellar lines calculated from Cen A (Turner et al. 1997, van den Bergh 1976) and from M31 (Irwin & Sarazin 1998), an energy line contributed to thermalization and gravitational heating, and a line from supernovae heating.

The X-ray luminosity of the brightest galaxies can be compared to the maximum amount of energy expected from gravitational energy release (L_{grav}) or supernovae (L_{SN}). We find $\log L_{grav} = 23.57 + (5/3)\log L_B$ assuming that gas falls nearly to the center of the galaxy before cooling (Canizares, Fabbiano, & Trinchieri 1987; Dressler 1984), and $\log L_{SN} = \log L_B + 30.22$ using a supernova rate given by Turatto et al. 1994. Both L_{grav} and L_{SN} may contain uncertainties of a factor of around two (see Brown 1998).

The slope of the relationship between L_X and L_B is potentially quite important and has been the subject of much previous discussion. If we exclude NGC 5102 (where the X-ray emission is consistent with a stellar origin), the $\log L_X$-$\log L_B$ relationship has a slope of 2.72±0.27, using an orthogonal linear regression bisector method (OLS bisector; Feigelson & Babu 1992); there is considerable scatter, approximately 1.5 dex in L_X for a fixed L_B. When the hard X-ray component from Cen A is subtracted, so that L_X is only from the hot gas, the relationship becomes steeper, with a slope of 3.03±0.32. This is much steeper than the slope of approximately 5/3 that is expected from the model where gas is thermalized, remains bound to the galaxy, and falls inward.

The wide range of L_X for a given L_B and the steepness of the L_X - L_B relationship for the gaseous emission are inconsistent with the standard cooling flow model. We suggest a modification of the model that may help to resolve these problems. In this revised picture, environment plays a central role in determining the luminosity - galaxies are trying to drive galaxtic winds, but the visibility of the X-ray emission depends on whether the wind is stifled (pressure confined) by the ambient cluster or group medium. Observations support this in that the most X-ray luminous galaxies are generally associated with the richest environments, such as the Virgo cluster (NGC 4406, NGC 4472, NGC 4636, NGC 4649), the Fornax cluster (NGC 1399, NGC 1404), or in the centers of moderate richness groups (e.g., NGC 5846).

We find that many of these luminous galaxies are significantly hotter than T_σ, another inconsistency with the basic model (Figure 2). The slope of the $\log T_X$ - $\log T_\sigma$ relationship is 1.43±0.21, which is steeper than the nominal theoretical expectation ($T_X = T_\sigma$). Eight galaxies that are "too hot" relative to T_σ are NGC 1399, NGC 1404, NGC 1407, NGC 3923, NGC 4406, NGC 4472, NGC 4636, and NGC 5846. This list is nearly identical, with an overlap of 7/8 galaxies, to a list of the eight most X-ray luminous galaxies: NGC 1399, NGC 1404, NGC 1407, NGC 4406, NGC 4472, NGC 4636, NGC 4649, and NGC 5846 (in increasing NGC number). These overly hot temperatures would occur in a supernova-heated atmosphere confined by cluster or group medium.

There is a positive correlation between the L_X/L_B ratio and richness of environment (see Figure 3). Only X-ray faint galaxies are found in relatively isolated regions of space, whereas galaxies with the highest L_X/L_B ratios have many bright neighboring galaxies. Environment may have several effects on the hot gas content of a galaxy. In a very dilute surrounding medium, a supernova-driven galactic wind would occur (lowering the observed X-ray luminosity), but in a poor cluster (i.e., Virgo), the ambient medium may be adequate to pressure confine a wind, enhancing the X-ray luminosity of a galaxy. A competing process in richer environments is ram-pressure stripping, which would remove hot galactic gas, ultimately reducing its X-ray luminosity (Takeda, Nulsen, & Fabian 1984; Gaetz, Salpeter, & Shaviv 1987; Sarazin & White 1988). In very rich clusters, ram-pressure stripping should be the dominant

process, so X-ray emission from hot galactic gas may be unimportant.

The primary weakness of our suggestion lies with the metallicity, which is expected to be above the solar value given the observed supernova rates. The X-ray metallicities would suggest that the true supernova rate is 3 - 10 times lower than the published rates. An alternative explanation is that the observed supernova rates are accurate but that the metals are not mixed effectively into the hot galactic gas (see also Ciotti et al. 1991). Ineffective mixing of the metals would be necessary for our picture to remain viable. We look forward to the results of the ongoing supernova searches with CCD detectors, which should determine the observed rate to much higher accuracy.

We would like to thank a variety of people for valuable discussion: J. Irwin, J. Mohr, P. Hanlan, R. White, M. Loewenstein, G. Worthey, J. Parriott, M. Roberts, D. Hogg, and R. Mushotzky. Special thanks is due to the members of the *ROSAT* team and to the archiving efforts associated with the mission. Also, we wish to acknowledge the use of HEASARC and the NASA Extragalactic Database (NED), operated by IPAC under contract with NASA. Support for this work has been provided by NASA through grants NAGW-2135, NAG5-1955, and NAG5-3247; BAB would like to acknowledge support through a NASA Graduate Student Researchers Program grant NGT-51408.

References

Bregman, J. N., Roberts, M. S., & Hogg, D. E. 1992, ApJ, 387, 484

Brown, B. A. 1998, Ph.D. Thesis, University of Michigan.

Canizares, C. R., Fabbiano, G., & Trinchieri, G. 1987, ApJ, 312, 503

Ciotti, L., D'Ercole, A., Pellegrini, S., & Renzini, A. 1991, ApJ, 376, 380

Davis, D. S., & White, R. E. 1996, ApJ, 470, L35

Dickey, J. M., & Lockman, F. J. 1990, ARA&A, 28, 215

Donnelly, R. H., Faber, S. M. & O'Connell, R. M. 1990, ApJ, 354, 52

Dressler, A., 1984, ApJ, 281, 512

Faber, S. M., Wegner, G., Burstein, D., Davies, R. L., Dressler, A., Lynden-Bell, D., & Terlevich, R. J. 1989, ApJS, 69, 763

Feigelson, E. D., & Babu, G. J. 1992, ApJ, 397, 5

Forman, W., Jones, C., & Tucker, W. 1985, ApJ.

Gaetz, T. J., Salpeter, E. E., & Shaviv, G. 1987, 530

Hartmann, D., & Burton, W. B. 1997, "Atlas of (Neutral Hydrogen", Cambridge University Pres

Irwin, J. A., & Sarazin, C. L. 1998, ApJ, **499**, 65

Kim, D. W., Fabbiano, G., & Trinchieri, G. 1992, 134

Sarazin, C. L. 1990, in The Interstellar Medium i Galaxies, ed. H. A. Thronson, Jr. & J. M. Shull (D Kluwer), p. 201

Sarazin, C. L. & White, R. E. 1988, ApJ, 331, 102

Takeda, H., Nulsen, P. E. J., & Fabian, A. C. 1984. 208, 261

Tully, R. B. 1988, Nearby Galaxies Catalog (Camb University: Cambridge)

Turner, T. J., George, 1. M., Mushotzky, R. F., & N K. 1997, ApJ, 475, 118

van den Bergh, S. 1976, ApJ, 208, 673

White, R. E., & Sarazin, C. L. 1991, ApJ, 367, 476

Table 1. Galaxy Properties

Name	D (Mpc)	$\log L_B$ ($L_\odot$)	$\log L_x$ erg/s	T_σ (keV)	T_X (keV)	Name	D (Mpc)	$\log L_B$ ($L_\odot$)	$\log L_x$ erg/s	T_σ (keV)	T_X (keV)
N 0720	41.00	10.95	41.10	0.387	0.436*	N 4278	29.40	10.72	40-55	0.450	...
N 1316	28.44	11.34	41.08	0.403	0.351*	N 4365	26.66	10.79	40.48	0.390	0.200
N 1344	28.44	10.66	39.47	0.163	...	N 4374	26.66	10.99	41.09	0.524	...
N 1395	39.80	11.02	41.04	0.424	0.437*	N 4406	26.66	11.10	41.80	0.397	0.823
N 1399	28.44	10.88	41.44	0.610	0.944	N 4472	26.66	11.32	41.77	0.524	0.936
N 1404	28.44	10.74	41.27	0.323	0.557*	N 4494	13.90	10.20	39.28	0.300[a]	...
N 1407	39.80	11.16	41.34	0.517	0.913	N 4552	26.66	10.71	40.92	0.434	0.405*
N 1549	24.26	10.73	40.04	0.267	0.186	N 4621	26.66	10.78	39.79	0.367	...
N 2768	30.64	10.79	40.41	0.248	...	N 4636	26.66	10.96	41.81	0.232	0.717
N 3115	20.42	10.83	39.74	0.450	...	N 4649	26.66	11.14	41.48	0.740	0.823
N 3377	17.14	10.21	39.42	0.108	...	N 4697	15.88	10.58	40.13	0.173	0.206*
N 3379	17.14	10.49	39.78	0.257	...	N 5061	23.92	10.53	39.54	0.233	...
N 3557	47.98	11.10	40.61	0.541	...	N 5102	3.10	8.95	37.70	0.500[a]	...
N 3585	23.54	10.72	39.84	0.308	...	N 5322	33.22	10.80	40.11	0.319	0.205
N 3607	39.82	11.18	40.82	0.390	0.372	N 5846	46.72	11.26	42.01	0.491	0.733
N 3923	31.66	10.99	40.90	0.297	0.549	I 1459	44.50	11.14	41.19	0.601	0.414*
N 4125	39.72	11.16	41.01	0.332	0.283	N 7507	35-00	10.82	40.13	0.361	...

Distance, L_B, and T_σ derived from Faber et al. (1989) values. H_0 = 50 km/s/Mpc used throughout.
Starred values in the T_X column denote a two temperature fit value where the 2nd component is fixed at 2.0 keV.

[a]Adopted value for T_σ

Figure 1

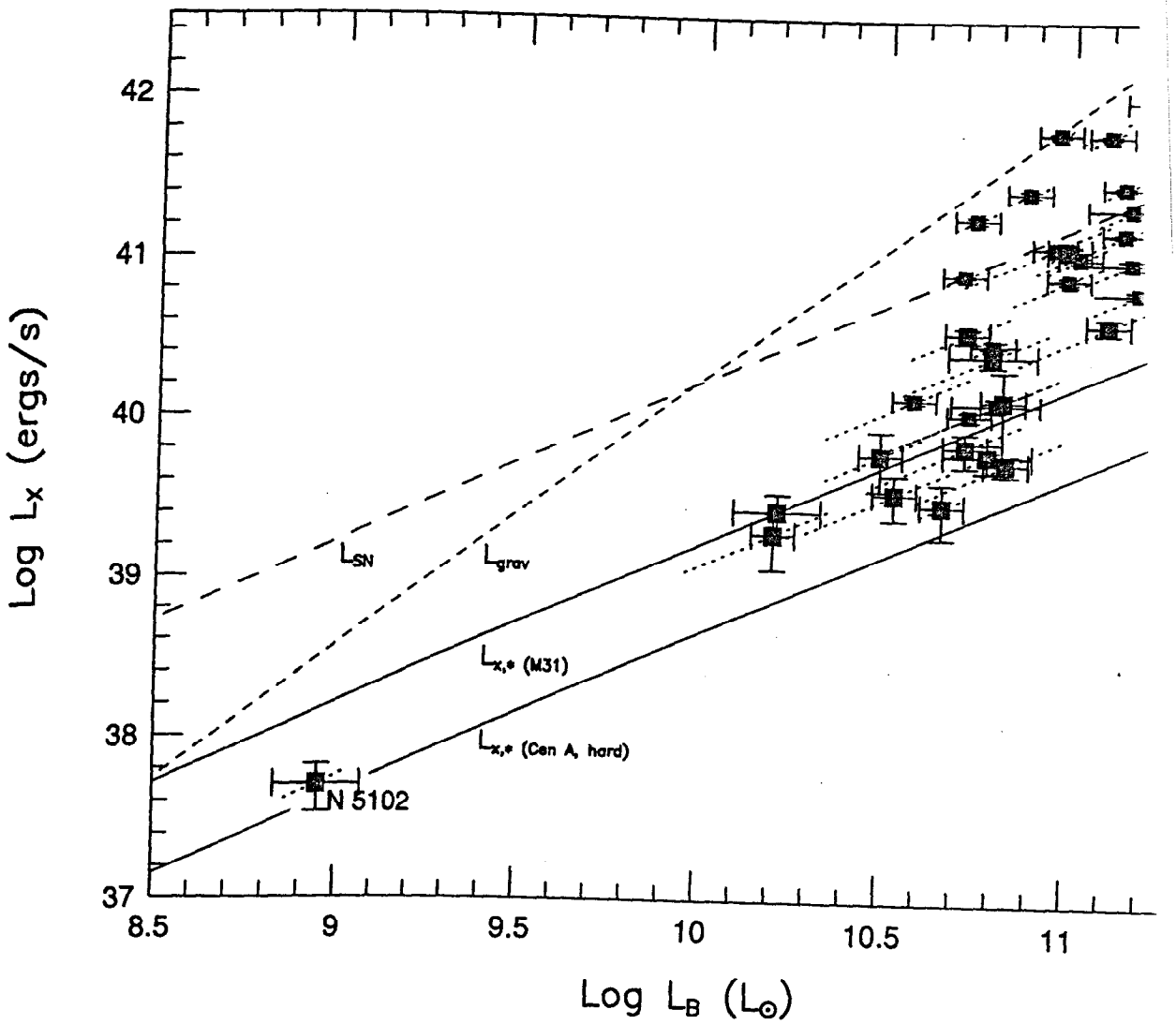

Figure 1. The 0.5-2.0 keV luminosities (in ergs s^{-1}) from the *ROSAT* PSPC and HRI instrument are given against their optical blue luminosities (in solar luminosities). The uncertainties due distances are shown as dashed lines of slope unity while errors due to distance-independent effects (e.g., photon statistics) are shown as the usual horizontal and vertical lines. The solid lines, $L_{x,*}$, are the stellar X-ray contributions as determined from M31 and the hard component Cen A, while the dashed lines labeled L_{SN} and L_{grav} represent the energy released from supernov or available from thermalization and gravitational infall.

Figure 2

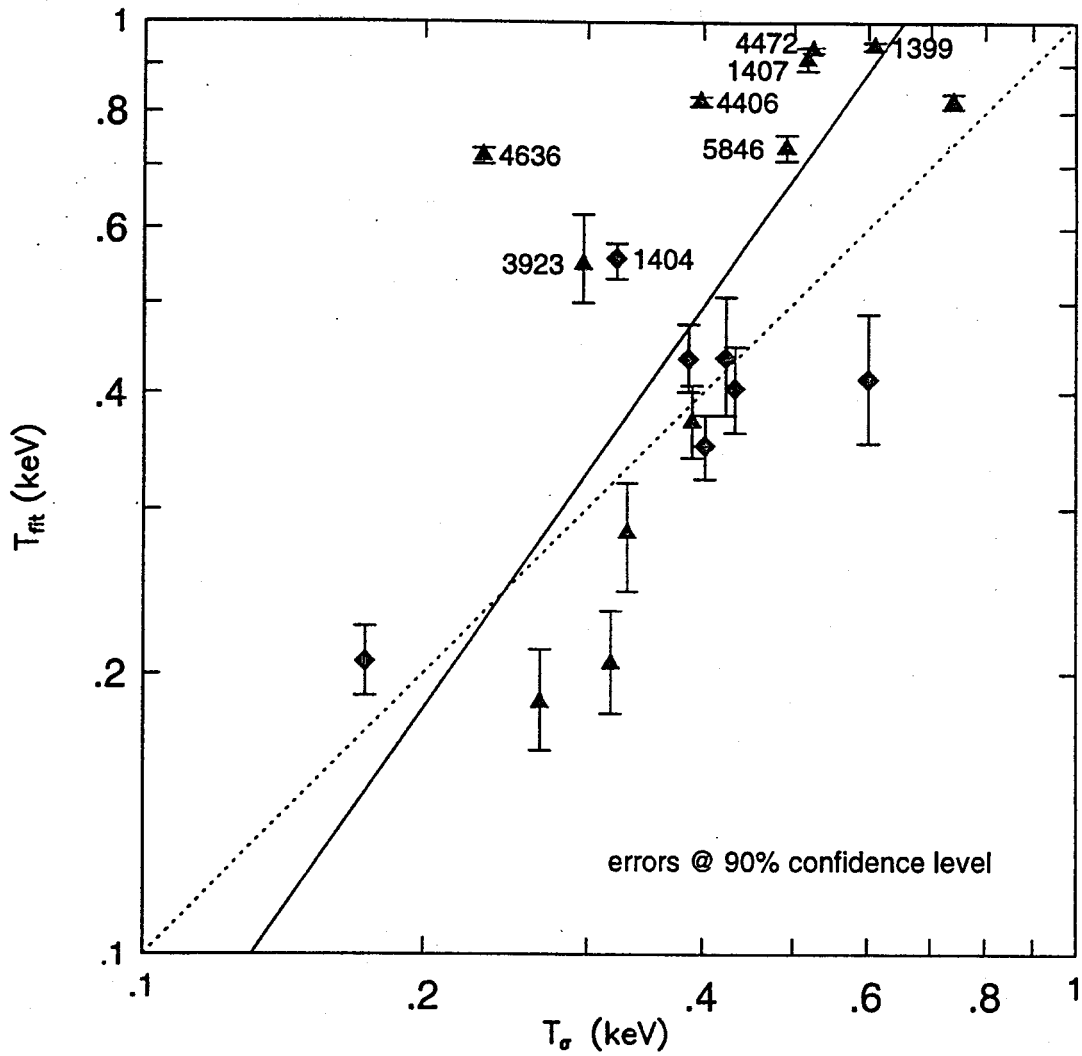

Figure 2. The gas temperature, as determined from fitting the X-ray spectral distribution vs the temperature corresponding to the velocity dispersion of the stars for high-count galaxies. The triangles denote single-temperature fits while the diamonds denote two-temperature fits. The uncertainties shown are 90% confidence errors. The dashed line denotes the $T_{fit} = T_\sigma$ relation. The solid line is the orthogonal linear regression bisector fit line.

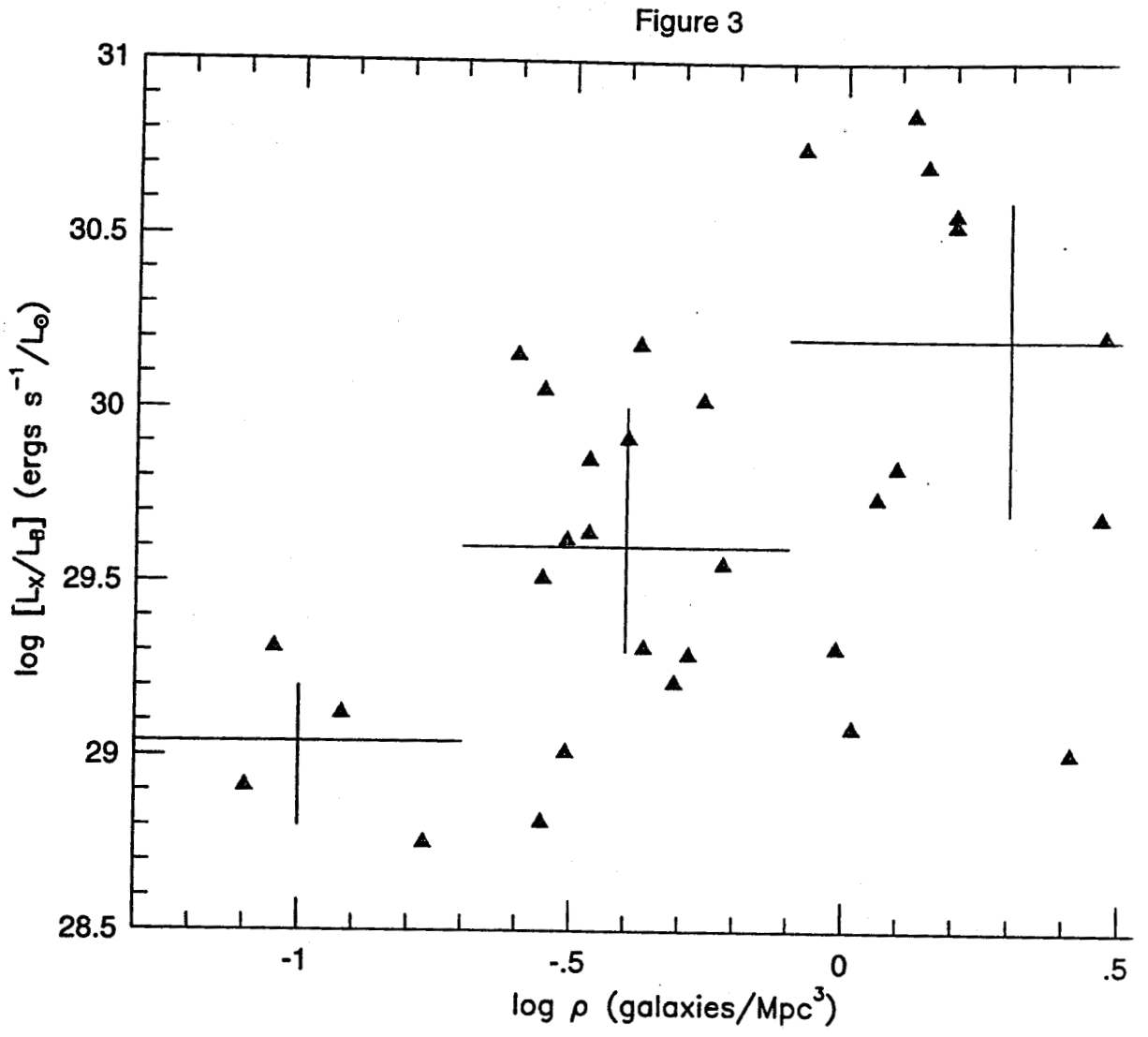

Figure 3. The ratio of the X-ray to optical luminosity vs. the local density of galaxies (per Mpc^3) brighter than -16mag in the vicinity of each galaxy (Tully 1988 values). The horizontal lines delineate the width of each bin and mark the median ration within each bin. The vertical lines are the magnitude of the upper and lower quartile values within each bin.

VIGILANTE: An Overview of a GPS Based ATR System

Kenneth A. Brown
Carl Christian Liebe
Suraphol Udonikesmaleel
Curtis Padgett
Michael Brenner
Ayanna Howard
Terry Wysocky
David Brown
California Institute of Technology

Steven Suddarth
Ballistic Missile Defense Organization

Abstract

The VIGILANTE project is a planned vision system capable of tracking and recognizing targets in real time, on a small airborne platform. The project consists of two parts, 1) the Viewing Imager/Gimballed Instrumentation Laboratory (VIGIL), which is an infrared and visible sensor platform with appropriate optics and 2) the Analog Neural Three-dimensional processing Experiment (ANTE), a massive parallel, neural based, high-speed processor.

The VIGIL platform is mounted on a helicopter equipped with Global Position System (GPS), Inertia Measurement Unit (IMU), gimbal, radio-link and anti-vibration platform. Also, a jet powered, radio controlled VIGILANTE Target Vehicle (VTV) has been manufactured and equipped with GPS. In the first stages of the project, the VIGIL system is used to acquire image sequences of the VTV for training and testing of the ANTE image recognition processor. Based on GPS and IMU input, the gimbal is pointed toward the VTV and acquires images.

This paper describes the VIGIL system in detail. It discusses position-based pointing, tracking algorithms and the alignment procedure. Test imagery and an evaluation of the system will be presented.

1. Introduction

Small air and space borne systems capable of autonomous acquisition and identification of hostile targets (e.g., cruise missiles, missile launchers etc.) will become an essential component of the Ballistic Missile Defense Organization's (BMDO) planned defensive mechanisms. Such Automatic Target Recognition (ATR) capability could greatly increase the capabilities of interceptors (for cruise and ballistic missiles), surveillance platforms (for missile launchers), and ground-based fire control.

The VIGILANTE project at Jet Propulsion Laboratory (JPL) [1] provides a low-cost

airborne platform that combines new sensors with advanced neural network processing algorithms for detection, recognition and tracking of missile threats. The project consists of two parts, the airborne VIGIL platform and the ANTE ATR processor.

VIGIL (Viewing Imager/Gimballed Instrumentation Laboratory) is a helicopter-based gimballed camera platform providing data acquisition for target training/ recognition experiments as well as testing of novel active and passive focal plane imagers. VIGIL provides realistic image conditions for airborne targets seen from above. To point the sensors toward the target (before the ANTE ATR becomes operational), both the helicopter and the VTV are equipped with GPS receivers, to provide the pointing information. ANTE (Analog Neural Three-dimensional processing Experiment) is a prototype image-processing/target-recognition computer architecture based upon technology developed under the ongoing 3 dimensional artificial neural network (3DANN) program. 3DANN is a sugar-cube-sized, low-power neural processor. It is capable of performing 64 simultaneous image convolutions with a 64x64-kernel size in real time [2] - [6]. This system will not be described further in this paper.

This paper describes VIGIL in detail. The algorithms for pointing the cameras towards the VTV are described. Also, the alignment procedures and noise sources are discussed.

2. Description of the VIGIL system

The VIGIL system consists of an airborne helicopter equipped with the gimbal sensor platform and a jet-powered target called the VTV.

THE VTV: A reusable, remote controlled target vehicle supports testing of VIGILANTE. Field testing of actual target signatures and backgrounds provides realistic scenarios needed to train and evaluate the ANTE system and its associated ATR algorithms. The VTV resembles a cruise missile, but is flown as a remote-controlled aircraft. An infrared signature is obtained from a Turbomin turbine engine producing 22 pounds of thrust for a flight time of about 15 minutes. The VTV is depicted in figure 1. It is 2.42 m has a 1. 18 meter wingspan and a ≈ 20 kilos.

THE AIRBORNE PLATFORM: The syste currently mounted on a Hughes 5C helicopter.[1] The helicopter and the depicted in figure 2.

As shown in figure 2, the VIGILANT consists of many sub-systems. In fi sketch of the system is shown. The section will describe the subsystem

QUANTOM WELL INFRARED PHOTO D (QWIP) is a 256x256 pixel, real-tin 120 Hz) IR sensor array. QWIP is a advancement compared to state-of- HgCdTe sensors. The sensor has an central wavelength detection capab 1 pm full width at half maximum, a design uses a random reflector on e to maximize light trapping. The QW are based on GaAs.

VISIBLE CAMERA: A color Cohu CCD pixel camera is used. The camera is with a Fujinon 300 mm zoom lens. I future, the CCD camera will be repla an active pixel sensor camera.

VIBRATION ISOLATION SYSTEM: The M Engineering Department, University Maryland has built an active/passiv stage vibration isolation control syst the project. The system operates on air mounts arranged in series with a stage of active electromagnetic actu active stage is used to isolate the ba excitation from the intermediate pla whose vibration is isolated from the system by the passive stage. The vib isolation control system is broken in parts. The first part is the two stage isolation control box and the other i control computer. The vibration isol is made of a composite material and the actuators, passive isolation, accelerometers and rate triad. The c computer contains the executable co logs the data and controls the I/O. Th two modes of operation for the syste first mode is a continuous operation that isolates the optical bench with S controlled gain parameters, which ha optimized for a specific camera confi

The other mode of operation is the data acquisition mode where the computer logs the output of the accelerometer and rate triads- Under most conditions, the vibration bench reduces vibration-related acceleration by a factor of ten.

Two Axes Gyro-Stabilized Gimbaled Mirror: The VIGILANTE gimbal is a two-axis gyro stabilized gimbal mirror constructed by Fraser-Volpe. The gimbal system consists of the gimbal electromechanical device and support electronics. The gimbal has an inner (horizontal) and outer (vertical) axis. The inner axis moves from -20 to +52 degrees and the outer axis moves +/- 45 degrees. The gimbal has two modes of operation: in position mode the mirror moves to the commanded position, in rate mode the mirror slews at the command rate. The gimbal has RS 232 interface to the telemetry system for commands and data. The gimbal position is read out automatically and transmitted to the ground station at ≈ 20 Hz.

Telemetry System: The VIGILANTE Telemetry system consists of three subsystems, as shown in figure 3. The first subsystem is the Ground Station, which receives all the data from the helicopter and the VTV. The second subsystem is the helicopter telemetry system consisting of two video down link channels (only one is shown in figure 3), command and data system, an attitude GPS system, gimbal and an IMU. The third subsystem is the GPS system on the VTV.

- The airborne telemetry subsystem for the VIGILANTE helicopter is comprised of. Two video transmitters (one is depicted in figure 3) that sends the images from the camera platform at 2.35-2.45 GHz down for ground-based recording and processing. A Communication Router (CR) distributes the commands from the ground to the airborne instrumentation and returns the GPS, Inertial Measurement Unit (IMU) and gimbal data to the ground station. The CR is a Motorola-based processor that receives commands from the ground and sends the data back at 57.6 K baud. The CR contains a 900MHz Freewave modem that sends and receives the data. The Attitude GPS system consists of a Pentium computer and 4 GPS receivers. The Attitude GPS system collects the GPS data from the 4 antennas, applies the received differential correction from the ground station and calculates a 4-antenna attitude solution (note the GPS antennas on figure 2). It then transforms the attitude solution from the GPS antenna reference frame to the aircraft reference frame. The attitude system then sends the attitude (pitch, yaw and roll), position of the aircraft (north, east, and altitude), velocities (north, east and down) and the GPS time to the ground control station. The Inertial Measurement Unit (IMU) is located on the optical bench so it is vibration isolated. The IMU transmits the accelerations and the roll rates in three axes through the CR at 50Hz.
- The ground station receives GPS data from a GPS antenna. It calculates the differential corrections and sends that information to the VTV and the helicopter. The ground station receives all the data from the aircraft and the VTV and sends it to VIGIL computer. The ground station contains two 57.6 K baud freewave modems and antennas (only one is show at figure 3), one for the VTV and the other for the helicopter command and data.
- The VTV hardware consists of a GPS antenna/receiver and a freewave modem/ antenna to receive the differential corrections and to send the position and velocity data to the ground station. The VTV calculates the latitude, longitude and altitude as well as the velocities east, north and down and transmits them to the ground station at 10Hz. The ground station calculates the relative VTV position with respect to the ground station.

3. Algorithms

The algorithms will evolve through two phases: In the early phases of the project, they will point the gimbal mirror toward the target, exclusively based on GPS information. The resulting acquired images will be used for training and evaluation of the ANTE recognition processor. Later in the project, the ANTE recognition processor will be included in a closed loop. Based solely on imagery, ANTE commands the gimbal mirror without

GPS information to demonstrate real time image processing capabilities. This paper will exclusively deal with pointing based on GPS information.

VIGIL's algorithms are based on four different coordinate systems (CS):

- The Ground Station Coordinate System (Ground-CS). The origin of the GROUND-CS is defined in the WGS-84[2] system. The geographical position of the GROUND-CS origin is irrelevant to VIGILANTE, as only the relative position of the helicopter and the VTV are important. The GROUND-CS is a Cartesian (flat earth) right hand coordinate system. The axes are defined as follows: The X-axis is pointing toward North. The Y-axis is pointing toward East and the Z-axis is pointing downwards. The units are in meters. Both the VTV and the helicopter positions are given in this coordinate system.
- The Helicopter body based CS (Helicopter-CS) is a right hand coordinate system. The origin is defined as being the right of the 4 GPS antennas on the helicopter. The X-axis is pointing forward on the helicopter. The Y-axis is pointing to the right (seen from above), and Z-axis is pointing downwards. The units are in meters. The IMU is aligned with the helicopter CS.
- The camera coordinate system (Camera-CS) is a right hand coordinate system. The origin is at the intersection of the optical axis and the CCD chip. The Z-axis is pointing backwards on the helicopter towards the gimbal mirror. The X-axis is pointing to the left (seen from above) and Y-axis is pointing down. The units are in meters.
- The gimbal-based coordinate system (Gimbal-CS) is a right hand coordinate system referring to the optical axis caused by the Gimbal mirror. The origin of the Gimbal-CS is at the center of the Gimbal mirror. The Gimbal-CS is defined as the CAMERA-CS translated to the Gimbal mirror center, and rotated ϕ degrees (right hand positive) around the Camera-CS z-axis. Successively the CS is rotated φ degrees (right hand positive) around the new y-axis. The units are in meters.

In figure 4 a sketch of the helicop CS's is shown.

The attitude of the helicopter is a combination of IMU and GPS attitu that is updated continuously. This the GPS attitude data has proven t unreliable, and hence the attitude made redundant by utilizing an IM algorithm for calculating the attitu in figure 6.

4. Alignment

There are position and angular unc in the mechanical mountings. The p uncertainty on the helicopter due t inaccurate measurements or mount estimated to be on the order of cent Assuming that the target is several h meters away from the helicopter, th uncertainties can be neglected. How there are 3 rotational uncertainties t not be neglected:

- Rotation from Ground-CS to the C antenna plane is very accurate. H the successive rotation to the Heli CS (described in 2. DESCRIPTION VIGIL SYSTEM) is based on a rotati provided by the user. This rotatio initially found using a compass an etc. It is estimated that the user, tr measure this rotation could introd error of several degrees in each ax
- The camera mounts are not precisi mounts. It is estimated that there n several degrees of error in each axi
- The commanded gimbal angles ma an offset; i.e. 0 degrees may not be pointing orthogonal to the helicopt estimated that this angle may have degrees of error in each axis.

A realistic model of the rotations (trans not included in this model) that the VT coordinates undergoes is sketched in fi

There are at least 8 unknown angles in model. It would be a very cumbersome procedure to determine and correct all angles. Besides, the configuration of the helicopter changes often, so a calibratio procedure that only takes minutes is absolutely necessary. The following

approximation has been made for making an easy calibration procedure: All misalignment rotations are collected in one single calibration rotation, which is supposed to counter rotate all the misalignments. This is depicted in figure 8.

The procedure for calibration is as follows: The tracking algorithm as displayed in figure 5-6 is initiated. The VTV is placed approximately orthogonal to the helicopter (by eyeballing). Most likely the gimbal is not pointed toward the VTV. Buttons can be used to adjust the calibration angles interactively until the VTV is in the center of the field of view. This procedure takes only a few minutes. It is estimated that the error introduced by this procedure is a fraction of a degree, which is acceptable for this experiment.

5. Experimental results

The VIGIL system has been debugged and tested at the Flight Research Inc., Mojave airport, CA. Initially the noise of a static scene is considered. This is the noise equivalent angle (NEA) of the system.

Position error on the VTV and the helicopter: The VTV and the helicopter positions are differential GPS positions at 10 Hz. In figure 9, the north/altitude of the VTV position is displayed for a static VTV. It is estimated that north/east noise (RMS) is less than a meter for the VTV and the helicopter, and that the altitude noise (RMS) is a couple of meters for both. It is expected that the noise would be larger in altitude due to the satellite geometry.

Attitude noise from the GPS system. The attitude of the helicopter is calculated at 10 Hz and based on updates from the 4 GPS antennas (shown in figure 2). Figure 10 shows the raw yaw and roll output of the GPS attitude. The noise (RMS) is significant lower than a degree. The roll angle is noisier than the pitch/heading angle because of a shorter baseline.

Unfortunately, the GPS attitude is not very stable. Hence, it is backed up by an IMU that is being integrated with 50 Hz. The algorithm was shown in figure 6. To illustrate the superiority of this approach, the raw yaw GPS attitude is shown together with the combined yaw attitude for a helicopter flight in figure 11.

All small individual noise contributions are added together in the noise on the gimbal angles. The two gimbal angles are shown in figure 12.

The NEA is only one element of the total pointing error budget. When things are moving, additional errors are introduced. At this early stage of the project it is impossible to make a complete error budget. However, a qualitative description of the source of additional error terms are given below:

- Nonlinearity due to collecting all alignment rotations in one alignment rotation: It is not mathematical correct to merge different rotations with different origins in the same rotation. This will introduce an error. It is estimated that this error is less than one degree.
- Flexin in the fuselage of the helicopter: During calibration, the helicopter is on the ground and the skids are carrying the weight of the helicopter. In flight, the rotor pulls the weight of the helicopter. This generates some flexing in the fuselage of the helicopter. This could amount to one degree.
- Propagation delay : There is a propagation delay in the radio modem at approximately 30 milliseconds. This means that GPS positions are old when they are received and, once the new gimbal angles are calculated it will take another 30 milliseconds before they reach the gimbal. This effect is somewhat mitigated by extrapolating the gimbal angles to the future. This effect is only significant when the VTV is making turns.
- Limited sampling frequencies: All signals are sampled. IMU is 50 Hz, GPS is IOHz, VTV position is 10 Hz and Gimbal position is 20 Hz. This limited sampling frequency will introduce an error when things are moving.

It has not yet been possible to make a thorough assessment of the equipment. However, during the first flights the equipment worked fine. The best way to illustrate the system capabilities is to show a series of selected pictures that was acquired of

a prototype VTV, with the VIGIL helicopter on the ground. The images are shown in figure 13.

6. Summary

This paper has been describing the VIGILANTE system. The flying target is equipped with GPS and radio modem. The helicopter is equipped with an active vibration isolated bench and a radio modem. On the bench, an IMU, gimbal, IR and visible camera are mounted. Outside the helicopter fuselage 4 GPS antennas are mounted. These provide a 4-antenna GPS attitude solution.

There are defined four coordinate systems, a ground based CS, a helicopter based CS, a camera based CS and a gimbal mirror based CS. The algorithms consist of successive coordinate translations and rotations of the target coordinates though the coordinate systems until the gimbal angles are calculated. The gimbal is finally commanded to a rate proportionally to the difference between the present mirror position and the calculated gimbal mirror position. The attitude GPS has proven to be unreliable, and is therefore backed up by the IMU.

There are multiple sources of mechanical misalignment on the helicopter. Positional errors are small compared to the target distance and are ignored. All rotational uncertainties are collected in one alignment rotation. It is possible to adjust the Euler angles of this alignment rotation iterative, until the target is boresighted. This procedure only takes a few minutes and introduces an insignificant error.

The system has been tested in the Mojave dessert. The random noise of the system is a fraction of a degree. The noise is larger when both the helicopter and the VTV are airborne simultaneous. With a target distance of ≈ 1 km and a field of view of 2.5 degrees, the VTV is in the field of view most of the time.

7. Acknowledgement

The research described in this paper was carried out by the Jet Propulsion Laboratory, California Institute of Technology, and was sponsored by the Ballistic Missile Defense Organization through an agreement with the National Aeronautics and Space Administration. Additional fundin by the National Physical Science C

References herein to any specific c product, process, or service by trac trademark, manufacturer, or other not constitute or imply its endorse the United States Government or th Propulsion Laboratory, California I Technology.

8. Notes

1 A dedicated VIGILANTE helicopter has b constructed, and will be used in later st project. The algorithms are constructed helicopter, assuming that the mirror is p the right. However, on the Hughes 500 h was necessary to mount the system poin left. Therefore there are small inconsiste between the images and the figures.

2 World Geodetic System 1984

9. References

1) S. Udomkesmalee et al: VIGILANTE: An A Sensing/Processing Testbed for ATR App SPIE Vol. 3069, p. 82-93.

2) S. Udomkesmalee, S. C. Suddarth: VIGILAN Ultrafast smart sensor for target recogniti precision tracking in a simulated CMD sc AIAA/BMDO Technology Readiness Confe Diego, August 18-22, 1997.

3) N. Alhambra, S. C. Suddarth, S. Udomkesn VIGILANTE Data Handling System: ASIM f Automatic Target Recognition. GOMAC'98 Systems and Their Applications, Arlingtor March 16-19, 1998.

4) A. Howard, C. Padgett, and C. C. Liebe: A r Neural Network for Automatic Target Dete appear in international Joint Conference Networks (IJCNN), May 1998.

5) C. Padgett and G. Woodward: A Hierarchic Automated Target Recognition for a Parall Processor. The 1997 IEEE International Sy on Computational Intelligence in Robotics Automation, p. 374-379, Monterey, July 1

6) C. Padgett, M. Zhu, and S. Suddarth: Detec orientation classifier for the VIGILANTE im processing system, Proceedings of SPIE Vol. 191-201. Editors Rogers, S. April 1997.

7) J. Werts. Spacecraft Attitude Determinatior Control. D. Reidel Publishing Co., MA, 1978

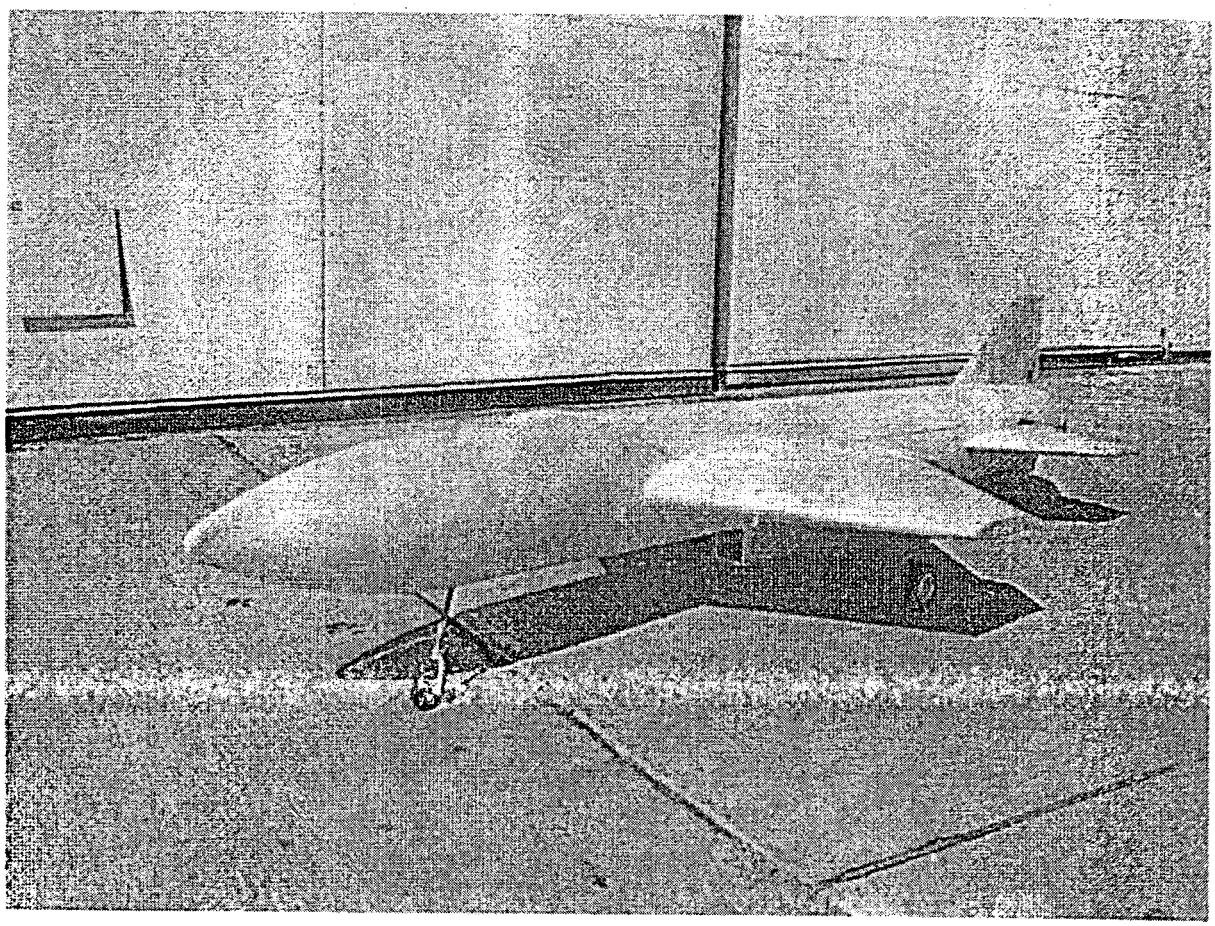

Figure 1. The VTV.